ChemComm

Cite this: *Chem. Commun.*, 2011, **47**, 3808–3810

www.rsc.org/chemcomm

COMMUNICATION

FITC-modified PPy nanotubes embedded in nanoporous AAO membrane can detect trace PCB20 *via* fluorescence ratiometric measurement†

Meiling Wang,[a] Guowen Meng,*[a] Qing Huang,*[b] Qiaoling Xu,[a] Zhaoqin Chu[a] and Chuhong Zhu[a]

Received 5th December 2010, Accepted 11th January 2011
DOI: 10.1039/c0cc05371f

A highly sensitive and selective fluorescence ratiometric sensor membrane for 2,3,3′-trichlorobiphenyl has been achieved, *via* depositing polypyrrole nanotubes (PPyNTs, the fluorescence indicator) in nano-porous anodic aluminium oxide (NPAAO) template and subsequently immobilizing fluorescein isothiocyanate (as an internal reference) onto the inner walls of the PPyNTs embedded in the NPAAO.

Polychlorinated biphenyls (PCBs) are man-made chemicals comprised of 209 congeners with 1 to 10 chlorine atoms attached to biphenyl, and they were once widely used for dielectric fluids in transformers, capacitors, coolants and plasticizers. Although the production of PCBs was banned in 1970s as they were recognized as carcinogens, PCBs still persist in the environment and can be found worldwide due to their chemical stability, difficult degradation and long-range transportation. They are classified into the category of persistent organic pollutants (POPs), being capable of bioaccumulating in humans and other animals, and biomagnifying in the food chain.[1,2] Therefore, regulation and remediation of PCBs has become an imminent task, and the detection of trace PCBs is especially emphasized.

Up to now, there are several analytical approaches to detection of PCBs, such as gas chromatography, immunoassay, electrochemical magneto-immunosensor, and microscale methods.[3] However, these methods have low sensitivity, and are generally expensive, time- and energy-consuming. In contrast, the analytical method based on fluorescence spectroscopy shows advantages of simplicity, rapidity and high sensitivity, and has already been used for the detection of saccharide,[4a] metal ions,[4b] and pyrophosphate.[4c] Recently, we successfully developed a sensitive and selective fluorescent membrane for rapid detection of trace PCB101 with a lower detection limit of 1 ppb, by simply immobilizing the fluorophore phenyl isothiocyanate onto nanoporous anodic aluminium oxide (NPAAO) template.[5a] However, in view of practical applications, it is still a challenge to measure intrinsic fluorescence intensity with satisfactory accuracy and repetitiveness, as both the external environment and the instrument itself can readily interfere with the fluorescence intensity. It was reported that fluorescence ratiometric sensing, in which the ratio of fluorescence intensities at two well-resolved wavelengths is evaluated as the measuring parameter, can improve the accuracy of the fluorescence detection.[5b] Herein, for convenient, accurate, reliable and reproducible fluorescence detection of PCBs, we utilized two fluorophores; namely poly-pyrrole (PPy, with high fluorescence quantum efficiency) as the fluorescence indicator of the target analyte 2,3,3′-trichlorobiphenyl (PCB20), and fluorescein isothiocyanate (FITC) as an internal reference. This allowed us to build a fluorescence ratiometric sensor membrane, consisting of PPy nanotubes (PPyNTs) immobilized with FITC on their inner walls and embedded in NPAAO (denoted as FITC@PPyNTs@NPAAO), for trace detection of PCB20. When photo-excited under two sources of excitation light, the FITC@PPyNTs@NPAAO membrane emitted light at two well-resolved wavelengths of 330 nm and 532 nm, respectively. The new FITC@PPyNTs@NPAAO membrane showed effective sensing to PCB20, in sub-ppb range with high selectivity, demonstrating a new design route for developing simple, low cost, reliable and reproducible PCB trace detection approaches.

The FITC@PPyNTs@NPAAO was fabricated as shown schematically in Fig. 1A (Part S1 in the ESI†). Firstly, PPy was deposited onto the inner walls of the NPAAO channels as PPyNTs (denoted as PPyNTs@NPAAO), by using negative pressure deposition (NPD) (ESI, Fig. S1†) with $FeCl_3$ as an oxidant. Then, FITC was immobilized onto the inner walls of the PPyNTs (denoted as FITC@PPyNTs) embedded in the NPAAO membrane *via* simple adsorption.

Scanning electron microscopy (FE-SEM, Sirion 200) top view observations on the bare NPAAO template (Fig. 1B, achieved at 27 V_{DC} and 3 °C in 3% sulfuric acid aqueous solution[6]) and the PPyNTs@NPAAO membrane (Fig. 1C) reveal that the NPAAO channel diameters reduced from about 40 to 20 nm after PPy deposition, indicating that PPyNTs were successfully deposited inside the NPAAO pores

[a] *Key Laboratory of Materials Physics, Anhui Key Laboratory of Nanomaterials and Nanostructures, Institute of Solid State Physics, Chinese Academy of Sciences, Hefei, 230031, China. E-mail: gwmeng@issp.ac.cn; Fax: +86-0551-5591434; Tel: +86-0551-5592749*
[b] *Key Laboratory of Ion Beam Bioengineering, Institute of Plasma Physics, Chinese Academy of Sciences, Hefei, 230031, China. E-mail: huangq@ipp.ac.cn*

† Electronic supplementary information (ESI) available: Experimental and discussion details, additional figures. See DOI: 10.1039/c0cc05371f

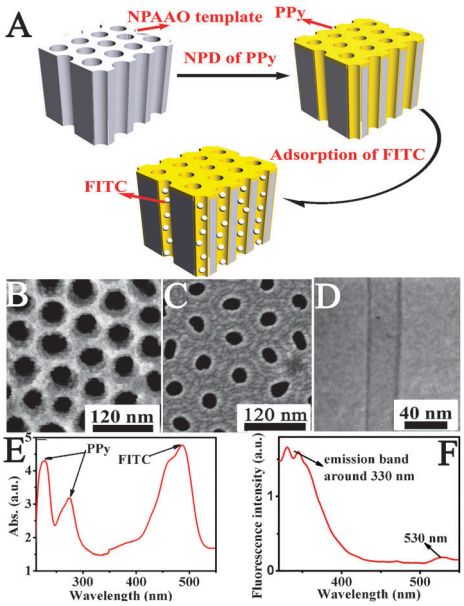

Fig. 1 (A) Schematic showing the fabrication process of the FITC@PPyNTs@NPAAO membrane. Close-up SEM top-views of (B) the bare NPAAO and (C) the PPyNTs@NPAAO membrane. (D) TEM image of a short segment of a representative PPyNT released from the template. (E) UV-vis and (F) fluorescence spectra of the FITC@PPyNTs@NPAAO membrane. (λ_{ex} = 300 nm).

(ESI, Fig. S2†). Transmission electron microscopy (TEM) observation of a representative PPyNT (Fig. 1D) demonstrates that the PPyNT has uniform diameter along its axial direction with its outer diameter being consistent with that of the nanochannels inside the NPAAO template.

UV-vis absorption spectrum (Fig. 1E) of the FITC@PPyNTs@NPAAO membrane (recorded *via* CARY-5E spectrophotometer) displays bands around 240–280 nm related to the aromatic ring interband π–π* transitions of PPy, and the absorption band of FITC at 490 nm, further confirming the successful loading of the dual-fluorophore FITC@PPyNTs onto the NPAAO template. The broadened absorption bands might be ascribed to the different conjugated lengths of PPy and the intermolecular interaction between PPy and FITC. The as-prepared FITC@PPyNTs@NPAAO membrane shows an emission band around 330 nm and a weak emission peak at 532 nm with excitation at 300 nm (Fig. 1F), demonstrating that it can be used as dual-fluorophore optical sensor by selecting right excitation sources. Details of the fluorescence spectra measurement conditions are given in Part S2 in the ESI†.

The responses of the FITC@PPyNTs@NPAAO membrane to varied concentrations of PCB20/n-hexane solutions are shown in Fig. 2A. It can be observed that the fluorescence intensity of the PPy (at 330 nm) decreases steadily with PCB20 concentration. If the ratio of the fluorescence intensities is defined as α:

$$\alpha = \frac{I_{330}}{I_{532}} \qquad (1)$$

where I_{330} and I_{532} are the fluorescence intensities of PPy and FITC, respectively; when the membrane is immersed in PCB20 solutions, it decreases steadily with PCB20 concentration (Fig. 2B). It can be seen from Fig. 2B that the FITC@PPyNTs@NPAAO ratiometric sensor membrane shows a dynamic detection range from 0.1 ppb to 10 ppb with a detection lower limit of 0.1 ppb, given that the criterion of 10% fluorescence quenching is enough to define the sensitivity of the fluorescence ratiometric sensor membrane. For PCB20 concentration higher than 10 ppb, the titration curve reaches a plateau (Fig. 2B), being ascribed to the complete occupation of the interacting sites for pyrrole association with PCB20. As depicted in the inset of Fig. 2B, there exists an approximate linear relationship between α and [PCB20] over the range of 0.1 to 0.8 ppb with a correlated coefficient of 0.07 as shown in eqn (2), which can serve as a quantitative analysis basis for the determination of PCB20.

$$\alpha = 1.19 - 0.07[\mathrm{PCB20}] \qquad (2)$$

Sensitivity of a fluorescence sensor can be evaluated by the Stern–Volmer constant K_{sv}.[5b] For the FITC@PPyNTs@NPAAO membrane, K_{sv} can be obtained from the slope of its Stern–Volmer plot (Fig. 2C), *i.e.*, $K_{sv} = 2.96 \times 10^8\ M^{-1}$ (ESI, Part S3†). This value is 3–5 order of magnitudes higher than that of the early report.[4b] Higher K_{sv} suggests higher sensitivity,[4b] therefore the FITC@PPyNTs@NPAAO indeed shows the advantage of superior sensitivity.

The selectivity of the FITC@PPyNTs@NPAAO membrane to PCB20 was evaluated by recording its responses to other PCBs including 2,2′,4,5,5′-pentachlorinatedbiphenyl (PCB101), 3,3′,4,4′-tetrachlorobiphenyl (PCB77) and 2,4,5-trichlorobiphenyl (PCB29), and other POPs such as hexachlorobenzene (HB) and pentachlorophenol (PCP) (Fig. S3†). Fluorescence spectra (Fig. S4†) and typical histograms of α (Fig. 2D) revealed that when immersed in *n*-hexane or 50 ppb PCB101, PCB29, HB, and PCP solutions, α showed no significant changes while, when immersed in 50 ppb PCB77, it was enhanced by about 20%. However, α was decreased by more than 50% after the FITC@PPyNTs@NPAAO membrane was immersed in 50 ppb PCB20. This means that the membrane can be employed to distinguish PCB20 selectively.

As the evaluation of the fluorescence intensity ratio of the two types of dye molecules can minimize experimental errors, this fluorescence ratiometric approach can provide reliable and reproducible measurements in PCB20 trace detection. Moreover, compared to small molecule-based sensor, fluorescence sensor based on PPy can achieve higher sensitivity due to the fluorescence signal amplification effect imparted by the PPy π-conjugated polymers. In order to show the structural and morphological superiority of our FITC@PPyNTs@NPAAO dual-fluorophore membrane, control experiments with PPy deposited on glass (denoted as PPy@glass) were conducted (the preparation of PPy@glass is given in Part S4 of the ESI†). The control experiments reveal that the FITC@PPyNTs@NPAAO membrane has the following advantages. *Firstly*, PPyNTs embedded in the nanochannels of the NPAAO template exhibit much stronger emission compared to that of the PPy@glass (ESI, Fig. S5A†). This can be explained as follows. When pyrrole is deposited inside the NPAAO channels and further polymerized into

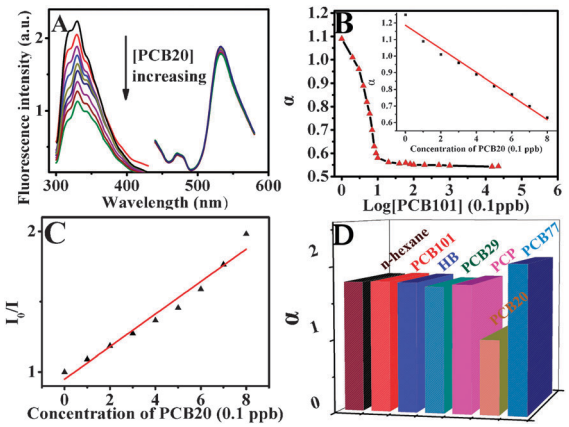

Fig. 2 (A) Fluorescence spectra and (B) titration curves of the FITC@PPyNTs@NPAAO membrane after being immersed in *n*-hexane, and 0.1–1, 2, 4, 6, 8, 10, 20, 50, 100, 1500, 2250 ppb PCB20/*n*-hexane solutions, respectively. (C) Stern–Volmer plot of the FITC@PPyNTs@NPAAO membrane as a function of different PCB20 concentrations. (D) Relative fluorescence intensity ratio of the FITC@PPyNTs@NPAAO membrane after being immersed in *n*-hexane, 50 ppb PCB101, HB, PCB29, PCP, PCB20, and PCB77, respectively. (λ_{ex} = 280, 420 nm for PPy and FITC, respectively).

PPyNTs, it exhibits different photophysical properties. The hydroxyl groups on the NPAAO pore walls may restrain the distortion of the PPy ring plane and increase steric hindrance, thus reducing nonradiative quenching caused by aggregated PPy phase. In addition, pyrrole immobilisation on the porous solid state blocked some of the nonradiative decay pathways by reducing the molecules' mobility and collision. All the above-mentioned will enhance the fluorescence quantum efficiency of PPy. *Secondly*, using NPD method will lead to enhanced PPy adhesion onto the NPAAO template, preventing leakage compared to PPy@glass (ESI, Fig. S5B and C†). *Thirdly*, inner pore walls of the FITC@PPyNTs@NPAAO can provide protection and reduce FITC photo-bleaching caused by long-playing irradiation, thus increasing its photo stability and reliability as an internal reference compared to that in solution (ESI, Fig. S5D and E†). *Fourthly*, the nanopores in the membrane can help to capture the analyte molecules; this nanoporous structure with ultrahigh surface-to-mass ratio provides extra interacting sites for PPy association with PCB20, all of which realize better contact and interaction between PPy and the PCB20, further enhancing the membrane sensitivity to PCB20. Thus the FITC@PPyNTs@NPAAO porous membrane shows an increase of about 4 order of magnitudes of K_{sv} compared to that of the imperforate PPy@glass, *i.e.*, 2.96×10^8 M^{-1} for FITC@PPyNTs@NPAAO and 8.728×10^4 M^{-1} for PPy@glass (the responses of the PPy@glass membrane to PCB20 are given in Fig. S5F of the ESI†). *Lastly*, ultrahigh surface-to-mass ratio of the porous FITC@PPyNTs@NPAAO fluorescence ratiometric sensor membrane can reduce probing-time for PCB20 (ESI, Part S5†).

The quenching of PPy emission by PCB20 is largely attributed to fluorescence/Förster resonance energy transfer (FRET) and electron transfer. Thus, two quenching mechanisms may occur: dynamic and static quenching. As there exists spectral overlap between the PPy emission and the PCB20 absorption in the wavelength range of 280–305 nm (ESI, Fig. S6†), once excited, energy transfer occurs when the two types of molecules get close to the proximity within the Förster distance (2–8 nm).[7a] As the nanopores of the dual-fluorophore membrane provide additional blockage for the movement of the trapped PCB20 during the molecular collision, PPy and PCB20 are more prone to get close to the proximity within the Förster distance and bring on FRET, verifying the contribution of dynamic quenching. On the other hand, exciplex may be formed between the excited PPy and PCB20 based on electron transfer from PPy to PCB20 *via* halogen-bonding.[7b] All these mechanisms work together and result in the large K_{sv} (10^8 M^{-1}).

In summary, a highly sensitive, selective and reliable fluorescence ratiometric sensor membrane of FITC@PPyNTs@NPAAO has been designed for the detection of trace PCB20. The membrane exhibits a dynamic detection range from 0.1 to 10 ppb with good selectivity. The mechanism of fluorescence quenching is due to both electron transfer and FRET that occurs in the proximity of PPy and PCB20. This work combined the advantages of the reliability of the fluorescence ratiometric sensor, fluorescence signal amplification effect of the π-conjugated polymers and the nano-structured ultrahigh surface-to-mass ratio of the FITC@PPyNTs@NPAAO membrane, showing a promising trace detection method for PCB20. The design concept applied in this work may open a door to trace detection of other POPs.

This work was financially supported by the National Basic Research Program of China (Grant 2007CB936601), the National Natural Science Foundation of China (50972145, 50525207 and 10975152), and the Key Innovative Project of Chinese Academy of Science (Grant KJCX2YWN341).

Notes and references

1 K. Borga, A. T. Fisk, B. Hargrave, P. F. Hoekstra, D. Swackhamer and D. C. G. Muir, *Environ. Sci. Technol.*, 2005, **39**, 4523–4532.
2 K. Borga, G. W. Gabrielsen and J. U. Skaare, *Environ. Pollut.*, 2001, **113**, 187–198.
3 (*a*) Y. Y. Shu, S. S. Wang, M. Tardif and Y. Huang, *J. Chromatogr., A*, 2003, **1008**, 1–12; (*b*) S. Bender and O. A. Sadik, *Environ. Sci. Technol.*, 1998, **32**, 788–797; (*c*) C. A. Richter, J. B. Drake and J. P. Giesy, *Environ. Sci. Pollut. Res.*, 1994, **1**, 69–74; (*d*) S. Centi, E. Silva, S. Laschi, I. Palchetti and M. Mascini, *Anal. Chim. Acta*, 2007, **594**, 9–16.
4 (*a*) S. Arimori, M. L. Bell, C. S. Oh and T. D. James, *Org. Lett.*, 2002, **4**, 4249–4251; (*b*) X. Wang, C. Drew, S. Lee, K. J. Senecal, J. Kumar and L. A. Samuelson, *Nano Lett.*, 2002, **2**, 1273–1275; (*c*) K. H. Chen, J. H. Liao, H. Y. Chan and J. M. Fang, *J. Org. Chem.*, 2009, **74**, 895–898.
5 (*a*) M. Wang, G. Meng, Q. Huang, M. Li, Z. Li and C. Tang, *Analyst*, 2011, **136**, 278–281; (*b*) F. Gao, L. Tang, L. Dai and L. Wang, *Spectrochim. Acta, Part A*, 2007, **67**, 517–521.
6 G. Meng, F. Han, X. Zhao, B. Chen, D. Yang, J. Liu, Q. Xu, M. Kong, X. Zhu, Y. J. Jung, Y. Yang, Z. Chu, M. Ye, S. Kar, R. Vajtai and P. M. Ajayan, *Angew. Chem., Int. Ed.*, 2009, **48**, 7166–7170.
7 (*a*) W. M. Shih, Z. Gryczynski, J. R. Lacowicz and J. A. Spudich, *Cell*, 2000, **102**, 683–694; (*b*) A. Karpfen, *Struct. Bonding*, 2008, **126**, 1–15.

